Nanosecond Magnetization Reversal in High Coercivity Thin Films

N. D. Rizzo, T. J. Silva, and A. B. Kos

***Abstract*—We used a wide-field Kerr microscope to measure magnetization reversal in high coercivity thin film media that were subjected to nanosecond field pulses. Coplanar waveguides were used as a field source. Two different samples of $CoCr_{10}Ta_4$ were measured. Sample A had a coercivity of 83 kA/m and sample B had a coercivity of 167 kA/m. For sample A, we find that after a step change in H, the magnetization initially relaxes exponentially with a time constant of 5 ns, and then relaxes logarithmically. We interpret this result as indicating a transition from dynamic reversal to thermal relaxation. In higher fields, the exponential relaxation time decreases according to $\tau = S_w/(H - H_0)$, where $S_w = 29.7$ μs · A · m^{-1} (373 ns · Oe). For sample B, only logarithmic relaxation is observed, implying that the dynamic magnetization response time is subnanosecond. We observe correlated regions of reversed magnetization in our Kerr images of sample A with a typical correlation length of 1 μm along the applied field direction. We propose a microscopic model of nucleation and growth of reversed regions by analogy to viscous domain wall motion.**

***Index Terms*—Coplanar waveguide, high speed magnetization reversal, Kerr microscope, thin-film media.**

I. Introduction

HIGHER data rates in disk drives require that magnetic recording media must respond faster. Typical data rates of 300–350 Mbit/s translate into a media reversal time of 2 ns or less. If the 40% annual growth in data rate continues, then the time per bit will be less than 1 ns in just two years [1], putting even more stringent demands on media reversal time. Several questions arise: Can the magnetic media respond in such a short time? What determines the media response time?

Previous experiments on particulate and continuous thin film media have demonstrated subnanosecond switching speeds [2]–[5]. However, the shorter media reversal times come with a cost: the coercivity is higher when reversing media at nanosecond time scales compared with reversal times of seconds. This increase in coercivity is the result of less thermally-assisted magnetic reversal occurring over the shorter time scales [6]. Eventually, the desired time scale for magnetic reversal may be even less than the average magnetization response time to thermal fluctuations τ_0. In addition, the magnetization M has a dynamic response time τ in an applied field H *independent* of thermal effects. Intuitively, one expects that a larger H will apply a larger torque $T = M \times H$, thereby reducing τ. However, the H applied by a write head cannot be increased without bound. Thus, the measurement and understanding of τ and τ_0 may play a critical role in maintaining projected increases in data rate.

In this paper, we report on the measurement of magnetization response times in thin films of sputtered $CoCr_{10}Ta_4$. The experiment used a Kerr microscope to quantify the magnetization reversal occurring in the media after exposure to pulsed fields that were nanoseconds in duration. Two samples were measured having remanent coercivities of $H_{cr} = 83$ kA/m (1040 Oe) for sample A and $H_{cr} = 167$ kA/m (2100 Oe) for sample B.

We find that for sample A, after a step change in H, the magnetization relaxes exponentially with a response time of $\tau = 5$ ns in fields insufficient for saturation. In higher fields, τ depends inversely on H. We observe an abrupt transition from the exponential response for pulse duration $t_p < 10$ ns, to logarithmic relaxation for pulse duration $t_p > 10$ ns, corresponding to the onset of thermal switching. The exponential response and the sharp demarcation with thermal relaxation are explained using concepts from nonequilibrium statistical mechanics. Kerr images of the media reveal correlated regions of reversed magnetization, suggesting a microscopic picture of magnetization reversal that consists of random nucleation and growth of reversed regions. This microscopic picture accounts for the macroscopic exponential magnetization response and the field dependence of τ.

For sample B, after a step change in H, only logarithmic relaxation is observed, indicating that the magnetization response time is subnanosecond. For this media, the length of the correlated regions of magnetization are smaller than the resolution limit of the microscope. The faster response time for media with smaller correlation lengths is consistent with our microscopic picture of magnetization reversal.

II. Experimental Technique

The experimental setup is shown in Fig. 1. The large field pulses were created using a coplanar waveguide [7], along with a high voltage pulse generator. The pulse generator was used to send nanosecond current pulses through the waveguide and produce in-plane magnetic field pulses directly above the center conductor.

For sample A, the data were acquired using a commercial pulse generator with a maximum pulse amplitude of 200 V. The rise time and fall time (10–90 criterion) of this pulse generator were approximately 2 ns, which allowed a minimum pulse duration of 2 ns, full-width-at-half-maximum (FWHM). Pulse duration for these experiments was always derived using a FWHM criterion. For sample B, the data were acquired using a pulse

Manuscript received July 9, 1999. This work was supported by the NIST Advanced Technology Program. Contribution of the National Institute of Standards and Technology, not subject to copyright.

The authors are with the National Institute of Standards and Technology, Boulder, CO 80303 USA (e-mail: {rizzo; silva; kos}@boulder.nist.gov).

Publisher Item Identifier S 0018-9464(00)00440-4.

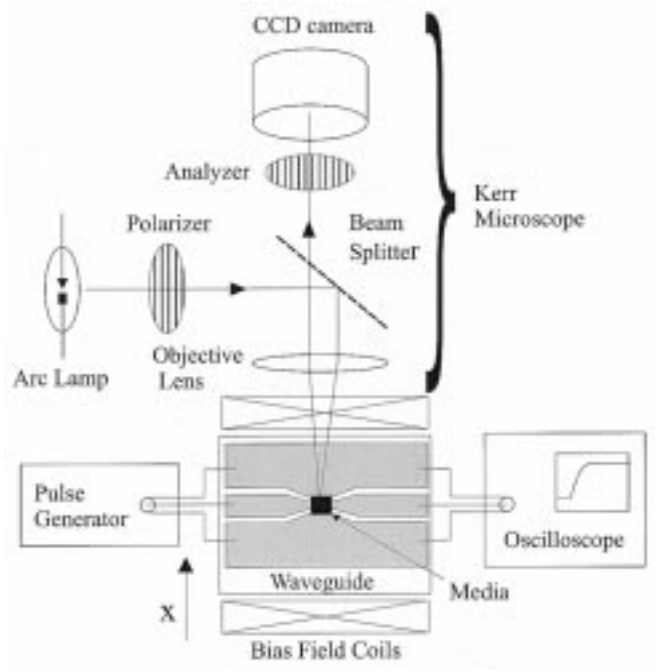

Fig. 1. Schematic of experimental setup.

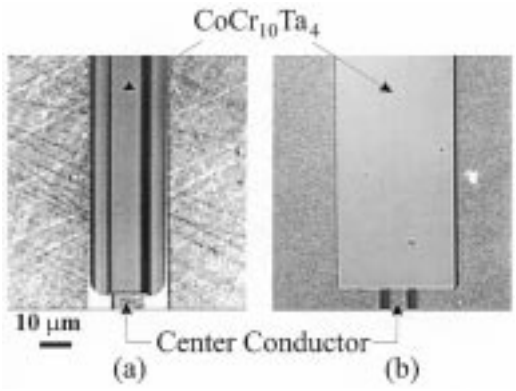

Fig. 2. Pictures of the $CoCr_{10}Ta_4$ media deposited on the center conductor of the coplanar waveguides. (a) Sample A: The waveguide is on an alumina substrate. A polyimide dielectric layer is between the media and the waveguide. (b) Sample B: The waveguide is on a sapphire substrate. A planarized SiO_2 dielectric layer is between the media and the waveguide. The scale bar applies to both pictures.

TABLE I
MAGNETIC PROPERTIES OF THE TWO $CoCr_{10}Ta_4$ FILMS

	H_{cr} (kA/m)	M_r (kA/m)	M_r/M_s
Sample A	83	490	0.90
Sample B	167	340	0.85

generator that we constructed with a 100 V maximum amplitude, a 0.6 ns rise-time, and a minimum pulse duration of approximately 1 ns.

The waveguide field was calculated assuming a uniform current density through the center conductor. The fields are equivalent to those described by the Karlqvist equations [8]. The field magnitude scales inversely with the width of the center conductor. For sample A, the width was 10.6 μm, so that the maximum waveguide field was 150 kA/m (1875 Oe) with a 200 V pulse amplitude. For sample B, the width was approximately 6 μm, so that the maximum waveguide field was 100 kA/m (1250 Oe) with a 100 V pulse amplitude. The calculated field values have been adjusted to account for resistive losses in the waveguide and spacing losses due to the dielectric layer.

The waveguide field pulse was combined with a much slower external bias field pulse (25 ms duration) provided by Helmholtz coils. The waveguide pulse was triggered near the maximum of the bias field pulse. The quasistatic bias field amplitude was constant for the duration of the waveguide pulse. The amplitude and duration of the bias field pulse and waveguide pulse were recorded using a high speed oscilloscope (1.5 GHz bandwidth, 8 GHz sampling rate).

The use of a bias field allowed larger total fields to be applied to the media. The bias field alone caused less than 4% magnetization reversal in the films. For sample A, the bias field amplitude was 66 kA/m (825 Oe). Hysteresis loops were measured both with and without a bias field for a pulse duration of 3.7 ns, and no significant difference was observed. For sample B, the bias field amplitude was 125 kA/m.

The waveguides were lithographically patterned from an Au film 0.75 μm thick on either an alumina substrate (sample A) or a sapphire substrate (sample B). To prevent voltage breakdown, the waveguides were covered with a dielectric layer approximately 0.8 μm thick. Sample A had a spin-on polyimide dielectric layer. Sample B had a SiO_2 dielectric layer that had been planarized using chemical-mechanical polishing.

Both samples consisted of a $CoCr_{10}Ta_4$ film (25 nm thick) on a Cr underlayer (25 nm thick). The films were sputter-deposited onto the region directly over the center conductor as shown in Fig. 2. For both samples, the substrate temperature during deposition was 250°C. In addition, during film deposition of sample B, a low energy ion beam was incident upon the substrate, giving a mill rate of approximately 0.01 nm/s. We measured the magnetic properties of codeposited samples, with the results shown in Table I.

To make electrical contact with the waveguide, we constructed microwave probes that were capable of sustaining the large voltage pulses without breakdown. The probe/waveguide combination has an intrinsic rise time of 0.5 ns, as determined by time domain transmission measurements with a 20 GHz sampling oscilloscope.

The magnetization reversal caused by a given field pulse was quantified using a wide-field magneto-optical Kerr effect (MOKE) microscope which was optimized for detecting longitudinal MOKE at a wavelength of 545 nm [9].

For each data point, the film was saturated in the positive x direction (shown in Fig. 1) using the external Helmholtz coils. Then, a digital image of the remanent state of the film was acquired using a 16-bit CCD camera. Next, a high speed field pulse was applied in the negative x direction. Finally, a second image of the film was acquired and digitally subtracted from the first to obtain the relative change in magneto-optic contrast. Examples of images obtained from pulsed media are shown in Fig. 3. Each difference image was averaged over an area (6 μm × 120 μm for Sample A, 3 μm × 120 μm for Sample B) to determine the average change in the remanent magnetization. We designate the remanent magnetization measured after a pulse of duration t_p as

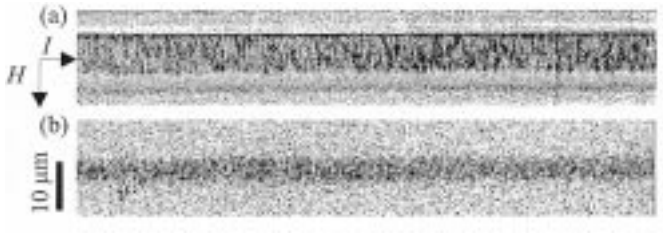

Fig. 3. Kerr microscope images of media for $M_r(t_p) = 0$ after a pulse duration of $t_p = 10$ ns. (a) Sample A and (b) Sample B. The waveguide current I and field H directions are shown. Sample A has visible regions of reversed magnetization. In Sample B the regions of reversed magnetization are too fine to resolve, which indicates lower media noise. The scale bar applies to both pictures.

$M_r(t_p)$, in contrast with the remanent magnetization measured after saturation, which is designated as M_r.

III. Results

We measured the magnetization response as a function of pulse duration t_p for a fixed pulse field amplitude H. (We use H to designate the total applied field amplitude, which is the sum of the bias field and the waveguide field.) We first present measurement results for sample A in Fig. 4. We observe a logarithmic decrease in $M_r(t_p)$ for all t_p at the lowest two fields. For higher H, a kink develops at 10 ns, indicating a sharp break in the magnetization decay rate. For the highest fields which cause saturation in $t_p < 10$ ns, the time required for saturation decreases with increasing field.

The kink is not an artifact of the pulse shape; we observe a similar break in slope when using a pulse generator with a rise time of 0.5 ns (see Fig. 5). The maximum pulse amplitude was 40 V for this pulse generator, so that a total field of $H = 90$ kA/m was the maximum that could be applied with a bias field of 66 kA/m.

For $t_p > 10$ ns, the magnetization decreases logarithmically in all fields, indicating the system is in metastable equilibrium with the applied field and is exhibiting thermal decay. The system is temporarily trapped in a local energy minimum, and is moving toward the global minimum through thermal activation over energy barriers that have a wide distribution of magnitudes. The probability of thermal reversal is given by the Arrhenius–Néel law [10]. The logarithmic decay rate (or remanent viscosity), $S_r \equiv \partial M_r(t_p)/\partial \log(t_p)$, is proportional to the irreversible susceptibility, $\chi_{irr}(t_p) = \partial M_r(t_p)/\partial H$, where $\chi_{irr}(t_p)$ was derived from the remanent hysteresis curve for $t_p = 10$ ns. This proportionality is a further signature of thermal relaxation [10], [11].

For $t_p < 10$ ns, we observe a large increase in the rate of change in magnetization as a function of t_p, particularly in higher fields. We interpret this increase as indicating dynamic or nonequilibrium relaxation. The kink at $t_p = 10$ ns then indicates a transition from nonequilibrium relaxation for $t_p < 10$ ns to metastable equilibrium and thermal decay for $t_p > 10$ ns. In other words, the magnetization has some finite response time before it can reach its new equilibrium value after an instantaneous change in the external field. We fit exponential functions

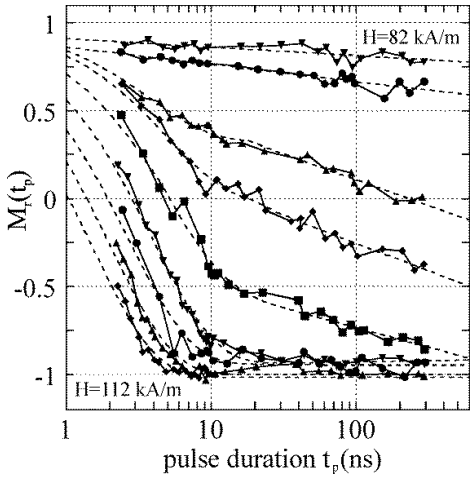

Fig. 4. Normalized remanent magnetization $M_r(t_p)$ of sample A versus pulse duration t_p for total field values $H = 82$, 86, 92, 94, 97, 102, 105, 108, 112 kA/m. The bias field was 66 kA/m. The dotted lines are fits of an exponential function for $t_p < 10$ ns and of a logarithmic function for $t_p > 10$ ns. The data for the two lowest fields are fit to a logarithmic function for all t_p.

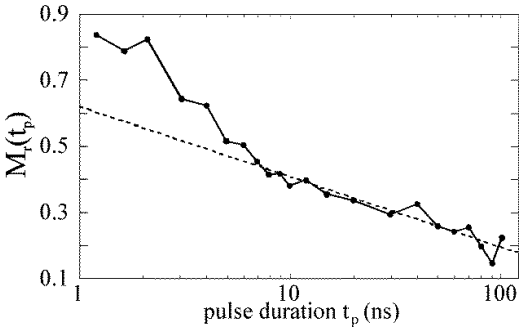

Fig. 5. Normalized remanent magnetization $M_r(t_p)$ of sample A versus pulse duration t_p for $H = 90$ kA/m. The bias field was 66 kA/m. The data was taken using a pulse generator with a rise time of 0.5 ns. The dotted line is a fit of a logarithmic function to the data for $t_p > 10$ ns.

to the data for $t_p < 10$ ns and logarithmic functions for $t_p > 10$ ns. The choice of exponential functions allowed a characteristic response time τ to be extracted from the data for a given field. The response times are shown as a function of H in Fig. 6.

The error bars represent 68% confidence limits as determined using constant χ^2 boundaries in the context of nonlinear least squares fitting [12]. The data for $H > 100$ kA/m were fit to the function $\tau = S_w/(H - H_0)$, with $S_w = 29.7$ μs $\cdot$ A $\cdot$ m^{-1} (373 ns $\cdot$ Oe). This inverse dependence of τ on H has been previously reported in studies of high speed magnetization reversal for both low and high coercivity materials [2], [13], [14]. The data for $H < 100$ kA/m were fit to a fixed value, with the result $\tau = 5$ ns. The independence of τ with respect to H has not been directly observed before in low or high coercivity materials.

The inability to previously observe this low field independence of τ was due to a different definition of switching times. If one defines the switching time as the pulse duration required to reduce the magnetization to zero, then a time constant cannot be defined for fields insufficient to demagnetize the sample. Our approach of explicitly fitting an assumed response function to the data allows us to determine a characteristic switching time for arbitrary levels of magnetization reversal.

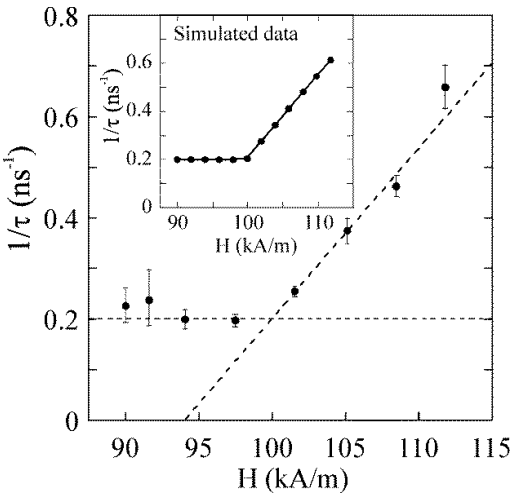

Fig. 6. Inverse response time $1/\tau$ versus applied field H for sample A as determined from exponential fits to the magnetization response for $t_p < 10$ ns. For $H > 100$ kA/m (1250 Oe), the function $\tau = S_w/(H - H_0)$ is fit to the data, yielding $S_w = 30\ \mu\text{s} \cdot \text{A} \cdot \text{m}^{-1}$ (373 ns · Oe). For $H < 100$ kA/m, a constant value is fitted to the data, yielding $\tau \approx 5$ ns. Inset: $1/\tau$ versus H as determined by exponential fits to simulated data that was generated assuming exponential magnetization relaxation, coupled with saturation effects.

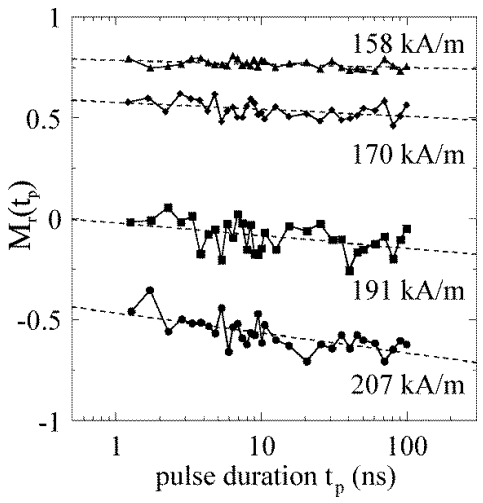

Fig. 7. Normalized remanent magnetization $M_r(t_p)$ of sample B versus pulse duration t_p for various total field values H. The bias field was 125 kA/m.

We have also measured the magnetization response of sample B as a function of t_p for a fixed pulse field amplitude H. The results are shown in Fig. 7. The bias field for these measurements was 125 kA/m (1575 Oe). Only logarithmic decay is observed, indicating that the magnetization is in metastable thermal equilibrium with the applied field for all pulse durations. We conclude therefore that the response time of this media is less than 1 ns. If exponential response is assumed, the upper limit on response time can be reduced to 0.5 ns; our signal to noise ratio is approximately 20 : 1 with this particular pulse generator, so that we should be able to resolve evidence of exponential relaxation for up to two time constants ($e^{-2} \approx 0.1$).

To summarize our results, we find that sample A has a characteristic magnetization response time of $\tau = 5$ ns that is independent of field when the field amplitudes are insufficient to achieve saturation within 10 ns. For higher fields, the response time is reduced in inverse proportion to the applied field above some critical value H_0, which presumably scales with the coercivity of the material. For sample B, the magnetization response time is subnanosecond.

IV. Discussion

A. Macroscopic Magnetization Response

Fine magnetic structure is evident in the Kerr images of sample A, as shown in Fig. 3. The spatial inhomogeneity of the magnetization response, along with its exponential relaxation in time, suggests that a statistical analysis is appropriate. Exponential relaxation is to be expected from nonequilibrium statistical mechanics in a linear response regime [15]. In this analysis, one assumes that $dM/dt = f(M)$, where $f(M)$ is some function of M. The dependence of $f(M)$ on higher order time derivatives of magnetization averages to zero due to the inherent randomness in the system. The linearized equation of motion for the magnetization response is then $dM/dt = -(M - M_a(H))/\tau_n$, where $M_a(H)$ is the asymptotic value of the magnetization determined by H, and τ_n is the ensemble average response time within the system. The solution of this equation is exponential with a time constant $\tau = \tau_n$. Exponential relaxation with a fixed time constant is an almost universal feature of highly disordered systems, in the limit of linear response [15]. If we use a linear approximation for the field dependence of M_r near H_{cr} with $M_a(H) = M_r - \chi^{(1)}(H - H_0)$, where $\chi^{(1)}$ is a constant, then the exact solution is,

$$M(t) = M_r - \chi^{(1)}(H - H_0) + \chi^{(1)}(H - H_0)\exp(-t/\tau_n). \tag{1}$$

The exponential response also implies that,

$$\chi_{irr}(t) = \left.\frac{\partial M(t)}{\partial H}\right|_t = -\chi^{(1)}(1 - \exp(-t/\tau_n)), \tag{2}$$

so that a decrease in $\chi_{irr}(t)$ is also associated with a finite magnetization response time. A decrease in $\chi_{irr}(t)$ at nanosecond time scales has been observed in pulsed field studies of particulate media and was also attributed to the onset of dynamic reversal [3].

The decrease of τ in higher fields is due to the nonlinearity of saturation. In fields large enough to cause saturation, the system responds exponentially with $M_a < -M_r$. Causality prevents the system from responding any differently, since it cannot "know" *a priori* that the applied field is sufficient to induce saturation. However, saturation abruptly cuts off the exponential approach to M_a when $M = -M_r$, so that the fitted exponential relaxation time τ is shorter than the relaxation time of the linear theory τ_n, as we show schematically in Fig. 8. In fact, one can solve (1) for τ such that $M(\tau) = (2e^{-1} - 1)M_r$ to show analytically that in the nonlinear regime the exponential fits will give $\tau \approx (M_r\tau_n)/(\chi^{(1)}(H - H_0))$.

The full field dependence of τ on H in both the linear and nonlinear regimes was also reproduced with a simple numerical simulation. Magnetization response was modeled as exponential with $\tau_n = 5$ ns, and nonlinear saturation at $M = -M_r$ was imposed. Exponential fits to the numerically generated data

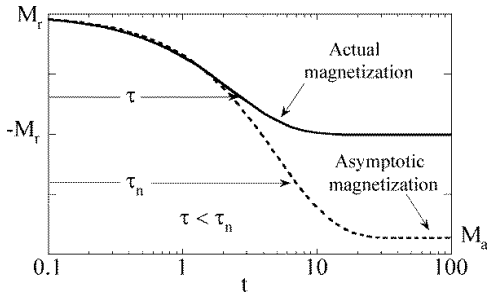

Fig. 8. Demonstration of how saturation causes a reduced time constant τ. The linear theory (dotted line) predicts exponential relaxation with time constant τ_n to a value $M_a(H) = M_r - \chi^{(1)}(H - H_0) < -M_r$. The magnetization initially follows the linear theory until saturation cuts off the response at $M = -M_r$. An exponential fit to the data will then yield $\tau < \tau_n$.

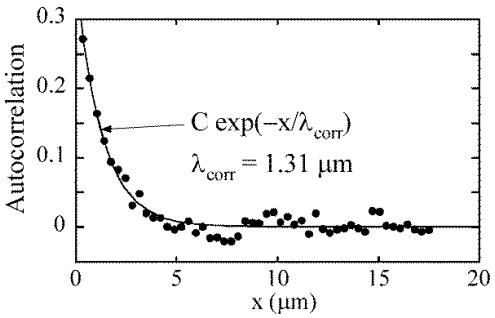

Fig. 9. The autocorrelation function derived from a Kerr image of sample A at $M_r(t_p) = 0$ for $t_p = 10$ ns. An exponential function was fit to the data to extract the autocorrelation amplitude C and the correlation length λ_{corr}.

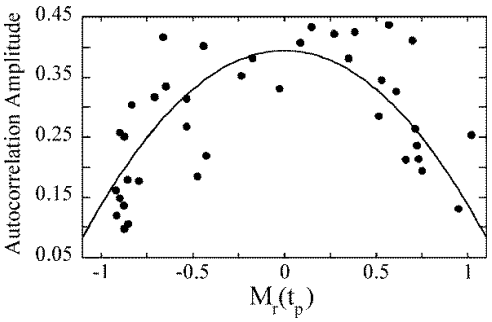

Fig. 10. The autocorrelation amplitude versus normalized remanent magnetization $M_r(t_p)$ derived from Kerr images of sample A for pulse duration $t_p < 10$ ns. A quadratic function is fit to the data, showing that the image noise is consistent with that of a two-state system.

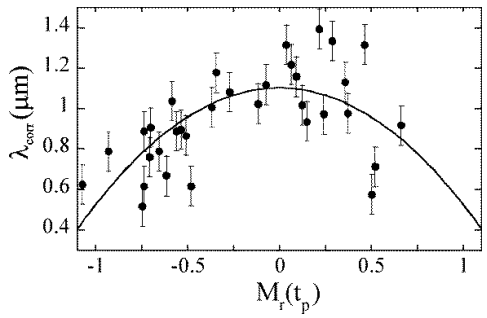

Fig. 11. Correlation length λ_{corr} versus normalized remanent magnetization $M_r(t_p)$ derived from Kerr images of sample A for pulse duration $t_p < 10$ ns. A quadratic function is fit to the data. This functional form is expected if the noise were generated by a random telegraph signal with different average lengths for "up" and "down" states given by $\lambda_{\rm up} = 1 - \lambda_{\rm down}$, and $\lambda_{\rm down} \propto M_r(t_p)$.

yields the results for τ versus H shown in the inset to Fig. 6, in excellent agreement with τ derived from fits to the actual experimental data.

The sudden transition between exponential and logarithmic response at $t_p = 10$ ns can be explained using Onsager's regression hypothesis (ORH). We use ORH to relate the nonequilibrium magnetization response to H and the magnetization response to microscopic thermal fluctuations while in metastable equilibrium. ORH states that, on average, the relaxation of microscopic thermal fluctuations while in equilibrium must obey the same equations that govern the macroscopic relaxation of a nonequilibrium state toward equilibrium [16], [17]. We conclude that the intrinsic linear magnetization response time after an instantaneous change in H (τ_n) *is the same as* the average relaxation time in response to thermal fluctuations (τ_0). Therefore, τ_n is the limit of thermal switching response.

B. Image Analysis

We performed image analyzes of the Kerr pictures of sample A for $t_p < 10$ ns, i.e., in the nonequilibrium regime. Regions of reversed magnetization are apparent in our Kerr images (see Fig. 3). We have calculated the average one-dimensional autocorrelation function for the images along the direction of the applied field H. A typical autocorrelation function is shown in Fig. 9, demonstrating the existence of a well-defined magnetic correlation length in the image. The correlation length transverse to the applied field was too small to be resolved. This suggests that switched regions grow along the applied field direction, presumably due to dipolar interactions. Exchange coupling would favor growth in the direction transverse to the applied field.

The autocorrelation function for each image was fit to an exponential $A(x) = C\exp(-x/\lambda_{corr})$. The amplitude C of the autocorrelation function is shown as a function of $M_r(t_p)$ in Fig. 10. C is proportional to the integrated noise power spectrum of the image [18]. The data are consistent with a quadratic dependence of C on $M_r(t_p)$, as would be expected for the variance of a two state system [8]. This is evidence that the primary source of correlated image noise is magnetic in origin, as opposed to an artifact such as surface topography.

The correlation length λ_{corr} for the images is shown as a function of $M_r(t_p)$ in Fig. 11. An approximate maximum in λ_{corr} occurs at $M_r(t_p) = 0$ and decreases as saturation is approached. A quadratic function was fit to these data, as well. Quadratic dependence of λ_{corr} on $M_r(t_p)$ is expected in the case of a random telegraph signal, where different average lengths for "up" and "down" states are given by $\lambda_{\rm up} = 1 - \lambda_{\rm down}$, and $\lambda_{\rm down} \propto M_r(t_p)$ [19]. The measured correlation length does not go to zero at $\pm M_r$ because of the finite optical resolution.

Similar behavior was previously observed in spin-stand measurements of thin film media, where the down-track magnetic correlation length extracted from dc erase noise had a maximum of 1.75 μm at $M_r(t_p) = 0$ and a minimum at saturation [20].

Numerical simulations also indicate that magnetic reversal in isotropic thin film media proceeds by nucleation and growth of reversed regions, predominantly along the direction of the applied field [21].

For sample B, the image analyzes show that $\lambda_{corr} \leq 0.5$ μm, which is the minimum correlation length that we could detect due to the finite optical resolution of our microscope.

C. Microscopic Model of Magnetization Reversal

We propose a microscopic picture of magnetization reversal that is consistent with the observed trends in the correlation length, the statistical nature of the reversal, and the dependence of τ on H. We assume that reversal occurs through nucleation and growth *along* the direction of the applied field. Growth continues until either the reversal is stopped by a region still exhibiting a finite net energy barrier, or coalescence with another switched region occurs. Growth is driven by a combination of the applied field and the internal demagnetizing fields produced at the ends of the reversed region.

The average equilibrium size of the reversed region depends linearly on applied field, so that $\lambda = \chi_\lambda(H - H_0)$, which is equivalent to again assuming $M_r(t_p) \propto (H - H_0)$. We also assume a random distribution of pinning sites so that a reversed region is pinned with a probability per unit length $1/\lambda$, which defines a Poisson point process of rate λ. The spatial magnetic noise generated from such a process is equivalent to that generated from a random telegraph signal, as described previously for Fig. 11.

The probability of a nucleated region expanding a distance x before being pinned when far from saturation is then $\exp(-x/\lambda)$. If an ensemble of N_0 regions nucleate, the number still growing after achieving a size x is $N = N_0 \exp(-x/\lambda)$. The growth of each region occurs with a velocity $v = \mu(H - H_0)$, where μ is the growth mobility, by analogy with viscous domain wall motion [22]. The ensemble average velocity is then $\langle v(t)\rangle = v \exp(-vt/\lambda)$, which gives the ensemble average domain size,

$$\langle l(t)\rangle = \int_0^t v(t')\,dt' = \lambda(1 - \exp(-vt/\lambda)). \qquad (3)$$

The magnetization response is then $M(t) = M_r(1 - 2\langle l(t)\rangle/\lambda_s)$, or more explicitly,

$$M(t) = M_r[1 - 2\lambda/\lambda_s + (2\lambda/\lambda_s)\exp(-vt/\lambda)], \qquad (4)$$

where λ_s is the average value of λ at saturation and the factor of 2 results from growth in both the positive and negative field directions. Therefore, the exponential relaxation time $\tau = \lambda/v = \chi_\lambda/\mu$ is independent of H until saturation occurs. As H increases further, $\lambda \rightarrow \lambda_s$, but v continues to increase without limit so that $\tau = \lambda_s/v = \lambda_s/\mu(H - H_0)$, or $\tau = S_w/(H - H_0)$, with $S_w = \lambda_s/\mu$. We note that this picture also predicts that size effects on S_w should be observable such that, when the film width $d \leq \lambda_s$, then $S_w \approx d/\mu$.

We can now use our model of reversal to derive values for the mobility μ as well as the damping constant α. We determine $\lambda_s \approx 1.4$ μm from the average correlation length for the Kerr images of sample A at $M_r(t_p) = 0$ (where we corrected for the finite optical resolution) and in the nonequilibrium regime ($t_p < 10$ ns). Using $S_w = \lambda_s/\mu$, we calculate $\mu = 0.047$ m$^2 \cdot$ s$^{-1} \cdot$ A^{-1} (3.8 m $\cdot$ s$^{-1} \cdot$ Oe^{-1}), a reasonable value when compared to $\mu = 0.2$ m$^2 \cdot$ s$^{-1} \cdot$ A^{-1} (16 m $\cdot$ s$^{-1} \cdot$ Oe^{-1}), a value recently obtained with a NiFe alloy [14].

Armed with a value for μ, we can estimate the damping constant α, again using the formalism of domain wall motion. The velocity of a domain wall is fundamentally limited by the reversal time of spins in the middle of the wall. Using the Landau–Lifshitz–Gilbert equation in a viscous flow approximation for a thin film, this reversal time is $\tau_{LLG} = \alpha/\gamma\mu_0(H - H_0)$ [23], [24]. The velocity of domain growth is then $v = a/\tau_{LLG} = a\gamma\mu_0(H - H_0)/\alpha$, where a is the domain wall width, that is, the length of material that is currently switching at any given moment. Therefore, we have $\alpha = a\gamma\mu_0/\mu$ [25].

We use the length of a demagnetization-limited bit transition as an estimate for $a \approx M_r\delta/2\pi H_{cr}$ [8], which gives $\alpha = 0.095$. This value is much larger than $\alpha \approx 0.02$, measured for single-crystal CoCrTa by ferromagnetic resonance [26]. A larger value for α is not surprising; the high degree of disorder in a polycrystalline film and the large amplitude of magnetic rotation for 180° switching both should enhance the dissipation of precessional energy into the thermal magnon bath.

According to the outlined model, the macroscopic magnetization response time $\tau = (\lambda_s/a)\tau_{LLG}$. For the case of sample A at saturation, $\lambda_s/a \sim 50$. Thus, the finite speed for the propagation of the microscopic switching event ultimately restricts the macroscopic response time τ to be well above the theoretical limit for coherent switching τ_{LLG}.

V. Conclusion

We have measured the response times for 180° magnetization reversal in high coercivity $CoCr_{10}Ta_4$ media. For sample A, the response time was 5 ns in fields insufficient to cause saturation. This response time may be decreased by applying larger fields such that saturation occurs. For sample B, the magnetization response time was less than 1 ns.

The relatively slow response times of sample A, compared with that expected for coherent rotation in a high anisotropy material, is a result of a characteristic length scale for magnetization reversal. The reversal occurs by nucleation and growth of reversed regions similar to viscous domain wall motion. Each grain can reverse coherently, but the time scale for complete reversal is set by the velocity of growth of the reversed region and the equilibrium size of the region, resulting in much longer response times than expected for coherent rotation alone.

This analysis implies that media with smaller magnetic correlation lengths (lower noise media) will reverse faster than media with larger correlation lengths (assuming all other things are equal, such as the growth mobility μ and the susceptibility χ). This may explain why sample B has a much smaller response time than sample A. The smaller magnetic correlation lengths for sample B as seen in Fig. 3, imply a shorter distance between nucleation sites (smaller λ_s), thereby reducing the reversal time. Our image analyzes established an upper limit on λ_{corr} of 0.5

μm, which implies that $\lambda_s < 0.4$ μm after correcting for the finite optical resolution of the microscope.

In the limit of completely decoupled single-domain grains, one should expect reversal times comparable to those for coherent rotation. However, such a benefit may result only at the expense of thermal stability; the fairly wide distribution of grain sizes in recording media implies that many small grains exist which are thermally unstable by themselves, but may be stabilized through interactions with other grains.

REFERENCES

[1] K. B. Klaassen, R. G. Hirko, and J. T. Contreras, *IEEE Trans. Magn.*, vol. 34, p. 1822, 1998.
[2] R. E. M. Thornley, *IEEE Trans. Magn.*, vol. 11, p. 1197, 1975.
[3] S. M. Stinnett, W. D. Doyle, O. Koshkina, and L. Zhang, *J. Appl. Phys.*, vol. 85, p. 5009, 1999.
[4] K. B. Klaassen and J. C. L. van Peppen, *IEEE Trans. Magn.*, vol. 35, p. 625, 1998.
[5] C. H. Back *et al.*, *Phys. Rev. Lett.*, vol. 81, p. 3251, 1998.
[6] M. P. Sharrock, *J. Appl. Phys.*, vol. 76, p. 6413, 1994.
[7] K. C. Gupta, *Microstrip Lines and Slotlines*, 2nd ed. Boston, MA: Artech House, 1996.
[8] H. N. Bertram, *Theory of Magnetic Recording*. Cambridge, MA: Cambridge University Press, 1994.
[9] B. E. Argyle, *Electrochem. Soc. Proc.*, vol. 90, no. 8, p. 85, 1990.
[10] R. Street and J. C. Wooley, *Proc. Phys. Soc. A*, vol. 62, p. 562, 1949.
[11] E. P. Wohlfarth, *J. Phys. F: Met. Phys.*, vol. 14, p. L155, 1984.
[12] W. H. Press, B. P. Flannery, S. A. Teukolsky, and W. T. Vetterling, *Numerical Recipes in C*. Cambridge, MA: Cambridge University Press, 1988, p. 551.
[13] W. D. Doyle, S. Stinnett, and C. Dawson, *J. Magn. Soc. Jpn.*, vol. 22, p. 91, 1998.
[14] R. H. Koch *et al.*, *Phys. Rev. Lett.*, vol. 81, p. 4512, 1998.
[15] L. D. Landau and E. M. Lifshitz, *Statistical Physics*, 3rd ed, E. M. Lifshitz and L. P. Pitaevskii, Eds, New York: Pergamon Press, 1980, pt. 1, p. 360.
[16] L. Onsager, *Phys. Rev.*, vol. 37, 38, p. 405, 2265, 1931.
[17] D. Chandler, *Introduction to Modern Statistical Mechanics*, New York: Oxford University Press, 1987, ch. 8.
[18] C. W. Helstrom, *Probability and Stochastic Processes for Engineers*, New York: Macmillan Publishing, 1984, p. 254.
[19] S. Machlup, *J. Appl. Phys.*, vol. 25, p. 341, 1954.
[20] H. N. Bertram, *IEEE Trans. Magn.*, vol. 26, p. 3129, 1990.
[21] J.-G. Zhu and H. N. Bertram, *J. Appl. Phys.*, vol. 69, p. 6084, 1991.
[22] C. Kittel and J. K. Galt, *Solid State Phys.*, vol. 3, p. 439, 1956.
[23] D. O. Smith, *J. Appl. Phys.*, vol. 29, p. 264, 1958.
[24] C. D. Olson and A. V. Pohm, *J. Appl. Phys.*, vol. 29, p. 274, 1958.
[25] J. F. Dillon Jr. and J. F. Dillon Jr., *Magnetism*, G. T. Rado and H. Suhl, Eds, New York: Academic, 1963, vol. III, p. 415.
[26] N. Inaba *et al.*, *IEEE Trans. Magn.*, vol. 33, p. 2989, 1997.